Acta Geodyn. Geomater., Vol. 21, No. 4 (216), 365–375, 2024
DOI: 10.13168/AGG.2024.0029

journal homepage: https://www.irsm.cas.cz/acta

ORIGINAL PAPER

DIFFERENCES IN CHEMISTRY AND MINERAL ASSEMBLAGES OF CZECH AND SLOVAK SERPENTINITE-TYPE ROCK AGGREGATES FOR MIXED RADIATION SHIELDING CONCRETE

Kamil SOBEK [1)*], Jitka KLAISNEROVÁ [1)], Claudia APARICIO [1)], Patricie HALODOVÁ [1)] and Petr ŠTEMBERK [2)]

[1)] *Department of Material Analysis, Research Centre Řež, Hlavní 130, 250 68 Husinec-Řež, Czech Republic*
[2)] *Department of Concrete and Masonry Structures, Faculty of Civil Engineering, Czech Technical University in Prague, Thákurova 7, 166 29 Praha 6, Czech Republic*

**Corresponding author's e-mail:* kamil.sobek@cvrez.cz

ARTICLE INFO

Article history:
Received 22 July 2024
Accepted 21 November 2024
Available online 4 December 2024

Keywords:
Aggregates
Serpentinization
Mineral chemistry
Spectroscopic techniques
Radiation shielding concrete

ABSTRACT

The chemistry and mineral assemblages of serpentinite-type rock aggregates used in radiation-shielding concrete vary, affecting the material's shielding effectiveness. These variations in aggregates result from different levels of serpentinization, leading to diverse compositions rich in serpentine, antigorite or lizardite minerals. These changes impact the overall radiation attenuation properties, differences in radiation-induced volume expansion, and concrete density. Understanding these distinctions is crucial when concrete mixes are tailored to specific shielding requirements in nuclear facilities. This ensures concrete-optimized radiation protection while maximising structural performance and durability. To identify such differences, a combination of Raman spectroscopy, large-area imaging and mapping using scanning electron microscopy coupled with energy-dispersive X-ray spectroscopy (SEM-EDS) and powder X-ray diffraction (PXRD) was performed to compare Czech and Slovak serpentinite rocks which were used in the construction of local nuclear power plants, which are still in operation.

1. INTRODUCTION

Concrete is the most commonly used material for radiation shielding due to its relatively low production cost and its efficacy in attenuating both neutrons and gamma rays. The main concrete structures in newly constructed nuclear power plants (NPPs) are designed to have a service life exceeding 60 years. Aging management studies of concrete used in existing NPPs have identified the most susceptible components and significant degradation factors that may impact the functionality of safety-related features (Torrenti and Nahas, 2010; Copinger et al., 2012; Remec et al., 2013; Bruck et al., 2019). The durability of concrete is mainly affected by mechanical stresses from structural loads, shrinkage and creep, thermal exposure/thermal cycling, enhanced carbonation, and the percolation of fluids through the concrete due to moisture gradient (Piotrowski, 2021). Prolonged exposure to high levels of radiation can cause changes in the microstructure of concrete, leading to its degradation. The radiation-induced volumetric expansion (RIVE) of aggregates significantly affects the structural integrity of radiation-shielding concrete, resulting in a significant reduction in the mechanical properties of the irradiated concrete, such as compressive strength and tensile strength and stiffness (Maruyama et al., 2017; Bruck et al., 2019; Khmurovska and Štemberk, 2021).

Serpentinite rocks are widely used for so-called serpentinite concrete, commonly used in the "dry" radiation shield of the Water-Water Energetic Reactor (WWER/VVER) type of pressurized water reactor (PWR) nuclear power plants built in the Russian Federation (Denisov, 2018) and other countries, such as the Czech Republic and Slovakia. In combination with heavyweight aggregates such as baryte, it improves radiation attenuation properties remarkably (Masoud et al., 2020). The presence of crystalline-bound water in serpentinite plays a crucial role in its effectiveness for radiation shielding, particularly for neutron attenuation. Serpentine minerals, primarily chrysotile, lizardite, and antigorite, contain approximately 13-14 % water by weight in their crystal structure (Coleman, 1971; Deer et al., 2009). This high structurally bound water content is particularly beneficial for neutron shielding, as hydrogen atoms are highly effective at moderating fast neutrons through elastic scattering interactions (Calzada et al., 2011; Abdullah et al., 2022). The bound water in serpentine's crystal structure, together with bound water in C-S-H gels of cement paste, provides a stable source of hydrogen that does not evaporate or migrate under normal conditions, ensuring long-term shielding performance (Rüpke et al., 2004; Sengupta et al., 2012).

Serpentinite forms from mafic or ultramafic rocks (such as dunite, harzburgite, or lherzolite) through a metamorphic process called serpentinization, which typically occurs under specific

Cite this article as: Sobek K, Klaisnerová J, Aparico C, Halodová P, Štemberk P: Differences in chemistry and mineral assemblages of Czech and Slovak serpentinite-type rock aggregates for mixed radiation shielding concrete. Acta Geodyn. Geomater., 21, No. 4 (216), 365–375, 2024. DOI: 10.13168/AGG.2024.0029

geological conditions involving water-rich environments and relatively low temperatures. Over time, the original minerals, such as olivine and pyroxene, are replaced by the serpentine group minerals. The extent of alteration during this metasomatic process affects the resulting mineral and chemical composition. The exact composition can vary depending on the parent rock and the specific conditions of serpentinization. Additionally, serpentinites may contain traces of elements such as nickel and chromium and common mineral impurities such as magnetite and Cr-spinels (Sobolev and Logvinova, 2005). While some of these impurities represent remnants of the original protolith, they impact the rock's mechanical qualities and stability, presenting noticeable issues for use in the NPPs. It has been described that several impurities in serpentinite rocks, such as dolomite, magnesite, calcite and particularly olivine, hornblende, and pyroxenes, can raise the radiation-induced alterations in the serpentinite concrete by 2-4 times (Denisov et al., 2012) and moreover by extending the service life of a nuclear power plant, the radiation changes in concrete may grow up to 6-12 times (Denisov, 2018). It was also shown that during the service lifetime, the serpentinite aggregate may affect the overall porosity of the concrete and thereby influence durability of the shielding (Dąbrowski et al., 2022).

This study aims to identify and define various serpentinite rocks based on different degrees of serpentinization and to determine the most appropriate serpentinite for use in a new generation of radiation-shielding concrete.

2. MATERIAL AND METHODS

2.1. SAMPLES PREPARATION

All studied samples were collected in an in-situ environment, either active or inactive quarries, corresponding to actual localities from where the aggregates were taken while the considered NPPs were constructed.

To characterise the microstructural features of the selected serpentinite aggregate samples, the test samples were prepared for SEM-EDS and micro-Raman analysis by processing them into polished epoxy-encased blocks/mounts. For the purposes of SEM-EDS analysis, the surface of the test samples was coated with an approx. 20 nm thick layer of carbon to suppress charging.

The samples were ground to a powder to identify individual phases in aggregate samples via PXRD. It is assumed that these materials will be tested after irradiation; therefore, we are investigating the optimal sample preparation method suitable for preparing active aggregates after irradiation in the environment of shielded glove boxes, following the procedure described in (Aparicio et al., 2024), where the studied material was ground in ethanol using an MM 400 oscillating mill in three stages.

2.2. CHARACTERISATION METHODS

Light optical microscopy (LOM) was used for primary characterisation of the studied aggregate samples. The Nikon Eclipse LV100N POL microscope was equipped with a 5-megapixel camera and image acquisition and processing software. The samples were photographed at either 5× (NA=0.15), 10× (NA=0.30), or 20× (NA=0.45) magnification.

The samples were analysed using a Tescan Mira GMU electron microscope for large-area imaging and elemental mapping, supplemented with an X-Max80N energy-dispersive analytical system and acquisition SW AzTec (Oxford Instruments). Data were acquired using an acceleration voltage of 15 kV, beam current of 3 nA, and approx. 1 μm spot size, where the total mapped area consists of segmented blocks with a size of 1000×1000 μm. For the quantitative analysis MAC 55 Reference Standard block containing pure elements and silicate minerals was used for standardization.

A confocal micro-Raman spectrometer, LabRam Evolution (HORIBA JOBIN YVON), equipped with a Peltier-cooled CCD detector and linked to an Olympus BX41 microscope, was used to collect single Raman spectra of selected minerals. The instrument was calibrated using the Rayleigh line using either 532 nm Nd: YAG or 473 nm diode-pumped solid-state laser. Data were collected in the 100–4000 cm^{-1} range utilising a diffraction grating with 600 grooves/mm, an entrance slit of 100 μm, a confocal hole of 200 μm and a 50× or 100× objective. The diameter of the spot for the measurement was ~1 μm. Data were processed with Seasolve PeakFit 4.1.12 and LabSpec 6 software. Band fitting was done after appropriate background correction, assuming Lorentzian–Gaussian band shapes.

The samples' diffractograms were collected by an Empyrean III diffractometer (Malvern-Panalytical), which is equipped with an X-ray lamp with a cobalt anode (Co-Kα, λ =1.789 Å, 40 kV, 40 mA, line focus) and a focusing mirror in the transmission mode setting. The range of 2 theta was from 5 up to 82°, with a step of 0.013° and a total measurement time of 2.5 h.

3. RESULTS AND DISCUSSION

3.1. PETROGRAPHIC AND MINERALOGICAL FEATURES

Serpentinite rocks from the Czech Republic (shortcut S1) are still mined today in the only serpentinite-active quarry in the vicinity of the town of Bernartice. The body of the deposit is stretched almost from east to west with a maximum length of about 3.5 km and a maximum thickness of about 900 m. The area around the deposit consists mainly of biotitic to sillimanite–biotitic paragneisses belonging to the Variegated Series of the Moldanubian Zone (Beneš, 1963). Serpentinite from Bernartice has a very dark green-black colour, fine-grained texture, and typical features on the exposed areas, indicating ongoing weathering processes (Fig. 1). This process is influenced by factors such as pH, temperature, and

Fig. 1 Specimens of serpentinite S1 taken from the site, together with a piece of magnesite vein. Scale for comparison (black & white rectangles equals 1 cm).

Fig. 2 Specimens of serpentinite S2 taken from the site, with intersecting light-coloured chrysotile veins. Scale for comparison (black & white rectangles equals 1 cm).

water availability (Olsen et al., 2023), resulting in the presence of secondary minerals. In addition to the serpentinite body, there are occurrences of peridotite relicts visible to the naked eye or veins with tremolite or magnesite present (Pauliš et al., 2010). Magnesite veins penetrating the deposit are also exceptionally thick (0.5–25 cm).

Serpentinite rocks from Slovakia (shortcut S2) come from an inactive quarry that is still accessible and lies in the vicinity of the town of Dobšiná. The body near Dobšiná belongs to serpentinized peridotites of the Mesozoic age. The oval lens of serpentinite, with the largest dimensions of about 700 m in the direction from east to west, is tectonically significantly broken. It is divided into several parts with typical fillings of relatively thick veins of white chrysotile asbestos (Hovorka et al., 1984, 1985). The colour is dark to light green (Fig. 2), rarely occurring as yellow-green. This represents a mineral composition dominantly rich in antigorite, chrysotile and lizardite. The occurrence of brucite, magnesite, calcite and other rare minerals is also caused by the weathering processes of the serpentine (Pauliš and Ďuďa, 2002). Dark to black rock parts occur in minor quantities and represent original lherzolites with minerals such as olivines, pyroxenes and spinelides.

The samples S2 were considerably texturally different from S1 even when observed with LOM. In the serpentinite S1, the main serpentine minerals appear to be relatively homogeneous, and the presence of other mineral inclusions, including extensive magnesite veins and cracks, is quite prevalent (Fig. 3a). Serpentinite S2 shows chaotically oriented minerals that are penetrated by chrysotile veins, with occasional cracks and the presence of other minerals (Fig. 3b).

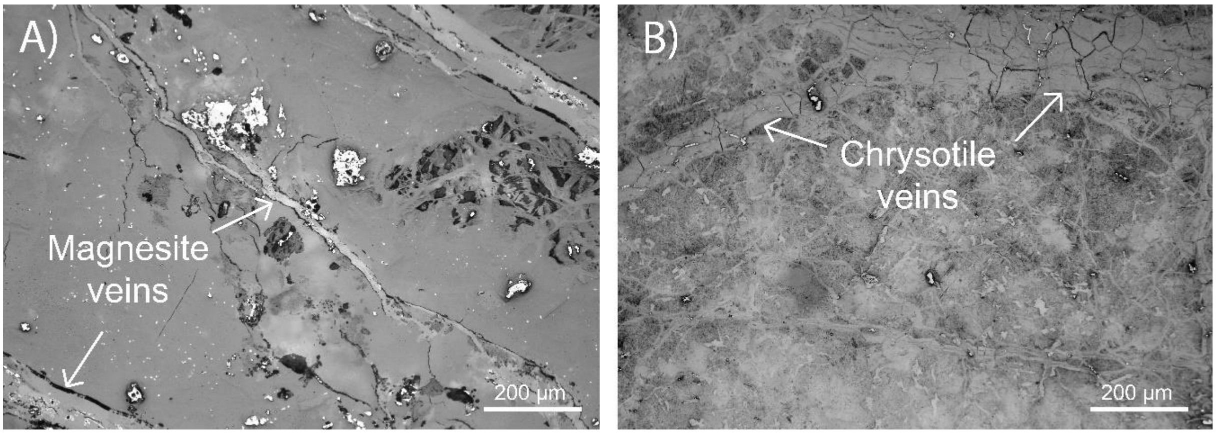

Fig. 3 Comparison of LOM images, in reflected light (10×), between a) Czech serpentinite (S1) with dominant magnesite veins and b) Slovak serpentinite (S2) with characteristic veins of chrysotile (asbestos).

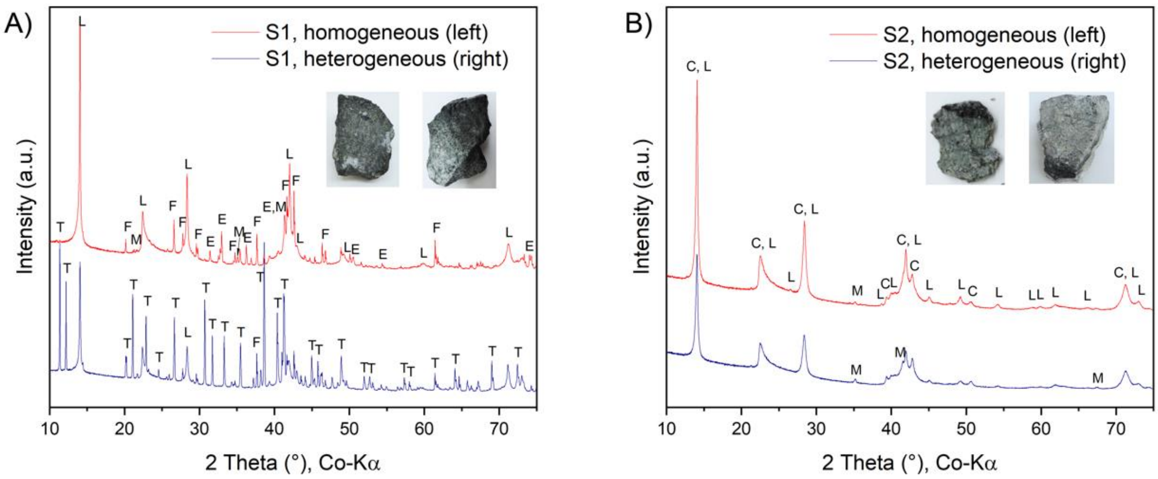

Fig. 4 Comparison of diffractograms of samples S1 (a) and S2 (b), the main phases are labelled with letters. C – chrysotile, E – enstatite, F – forsterite, L – lizardite, M – magnetite (spinel), T – tremolite.

3.2. PXRD AND MINERAL CHEMISTRY

The X-ray powder diffraction investigation of powdered bulk rock from two different localities allowed a comparison between Czech and Slovak serpentinite phase composition. The minerals detected in the S1 sample can be colour-differentiated into two parts, which were separated prior to the sample preparation for better recognition and phase identification. The brighter part (labelled as heterogeneous) of the serpentinite consists mainly of tremolite, a small amount of lizardite and traces of clinochlore. The dark part (labelled as homogeneous) has a different mineral composition; the main phases are lizardite and forsterite, pyroxene, magnetite (spinel), and clinochlore were also detected (Fig. 4a).

Similar minerals were identified in serpentinite originating from the S2 sample; however, they are represented in different amounts. The dominant light green part contains minerals such as chrysotile and lizardite. The dark parts of this sample also contain chrysotile and lizardite, while magnetite (spinel) was also detected (Fig. 4b).

Estimating the degree of serpentinization involves analysing changes in mineral assemblages and chemical compositions. As the process of serpentinization progresses, primary minerals such as olivine and pyroxene are gradually replaced by serpentine group minerals, with the highest degree consisting of only serpentine minerals, while also affecting the changes in Calcium (Ca), Magnesium (Mg), Iron (Fe) and Chromium (Cr) within the serpentinite deposit (Moody, 1976). Differences can be observed when we compare the bulk chemical composition of S1 and S2 (Table 1 or supplementary Fig. S1).

Mg is generally conserved during serpentinization, but its distribution shifts from olivine to serpentine minerals. Our values range from 39.08 to 41.79 wt.% MgO and correlate with SiO_2 content, with the remaining Mg bound to other mineral groups. Iron undergoes partial oxidation where Fe^{2+} from olivine changes to Fe^{3+} in magnetite. Iron is also present in other minerals that bind iron into the structure, including relict olivines where it remains in the Fe^{2+} form. Bulk values are almost similar with S1 – 5.15 and S2 – 5.08 wt.% Fe_2O_3. From Figure 5 it is noticeable that Cr forms discrete Cr-spinel phases (Hodel et al., 2017). Significant differences can be observed between the S1 – 1.02 and S2 – 0.29 wt.% Cr_2O_3 values, which also agrees with our observations,

Table 1 Bulk chemical composition of studied samples S1 and S2, results are shown in wt.%. *b.d.l.* = below detection limit.

	SiO_2	TiO_2	Al_2O_3	Cr_2O_3	Fe_2O_3	CaO	CoO	MgO	MnO	NiO	Na_2O	K_2O	H_2O
S1 Serpentinite	36.79	0.17	2.96	1.02	5.15	1.91	*b.d.l.*	39.08	0.13	0.21	0.94	0.24	11.39
S2 Serpentinite	43.85	*b.d.l.*	0.47	0.29	5.08	0.14	0.13	41.79	0.19	0.45	*b.d.l.*	*b.d.l.*	7.61

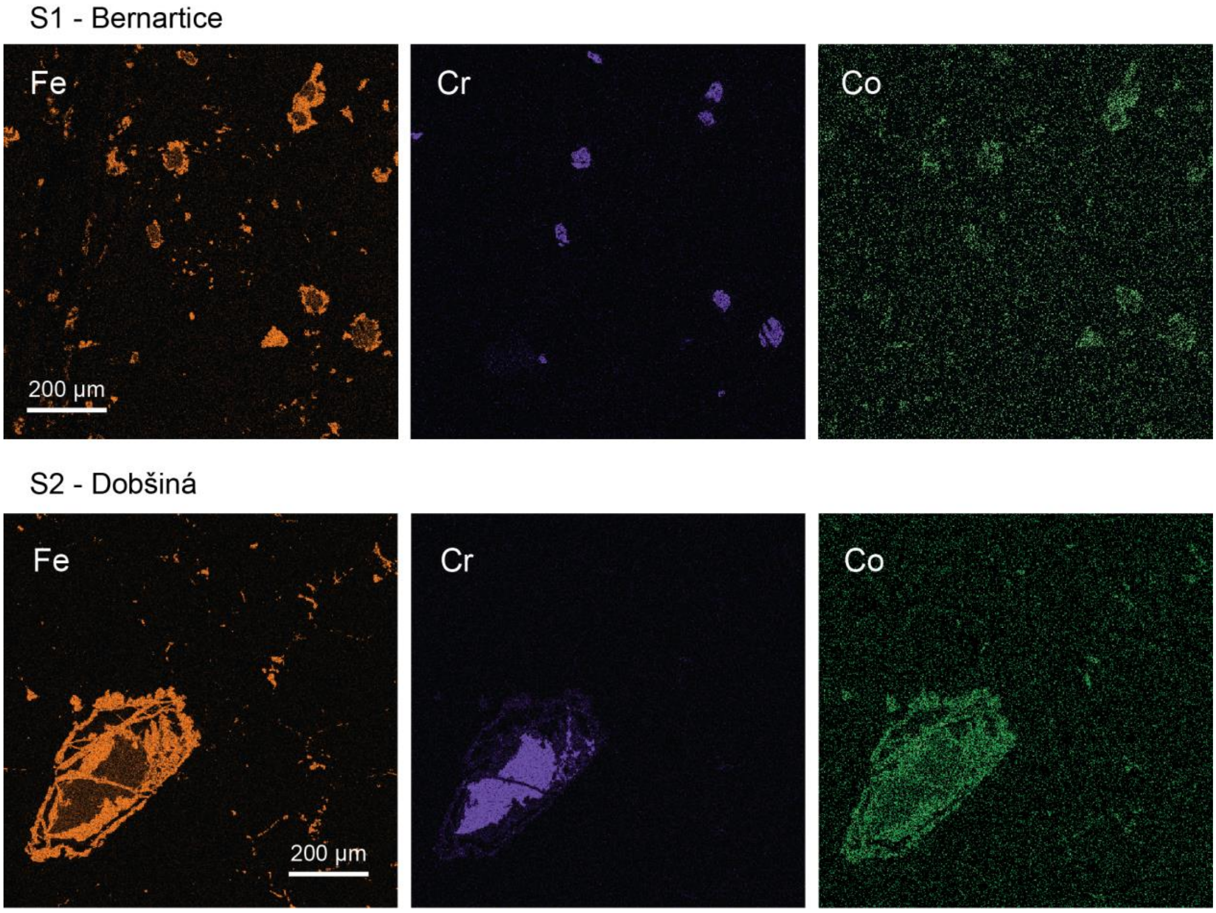

Fig. 5 EDS images of mapped areas in S1 (up) and S2 (down) for Fe, Cr and Co in relation to crystal grains of relict Cr-spinelides replaced by magnetite.

whereas in the case of S2, the presence of the Cr phase is much rarer. In both serpentinites, Cr concentrates in the core of the primary Cr-spinel phase, which is partly converted to secondary magnetite towards the rims (Figs. 5 and 6). Due to the natural abundance in the ultrabasic rocks, trace metals such as Cobalt (Co) or Nickel (Ni) were detected as well (Caillaud et al., 2009), where elevated values of these elements are present in S2 serpentinite. A rare mineral as the product of lateral weathering was detected in the case of Dobšiná in the form of closer unspecified Ni-smectite.

Cobalt is especially the most problematic since it leads to the formation of a relatively long-lived isotope of ^{60}Co that generates significant gamma radiation, which then causes the radiolysis of water in the serpentinites and cement and subsequent crack formation, thus reducing its attenuation and mechanical properties (Lavdanskij et al., 1989). Ca, K and Na are typically leached from the system, resulting in decreased values in the bulk content. Aluminium (Al) is dominantly concentrated in the mineral clinochlore or other minerals such as spinelides, antigorite and tremolite.

Quantitative assessments of serpentinization degree have been developed based on mineralogical-chemical changes, such as the magnetite proxy method (Toft et al., 1990) or the serpentinization degree index (Meer, 1994). Based on the elemental associations (Figs. 8 and 9), it is most likely evident that both bodies went through a different developmental stage of serpentinization, and it was most likely additionally affected by secondary alteration processes (Hodel et al., 2017). In the case of sample S1, considerable

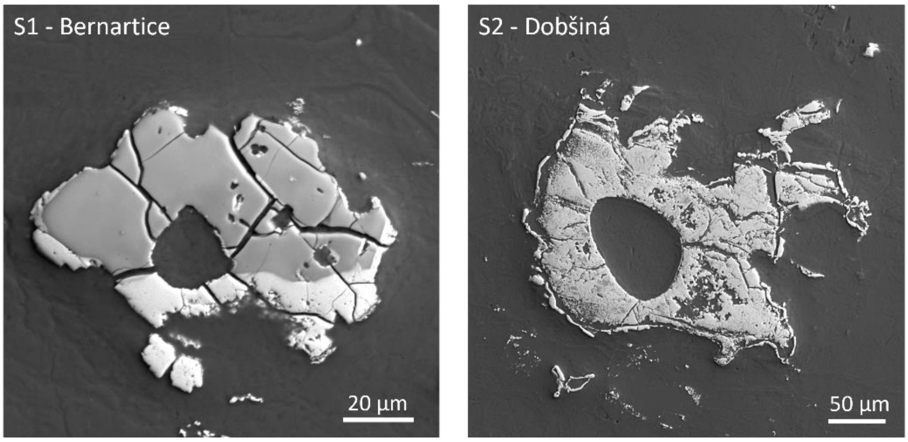

Fig. 6 BSE image of relict Cr-spinel grains partly replaced by secondary magnetite.

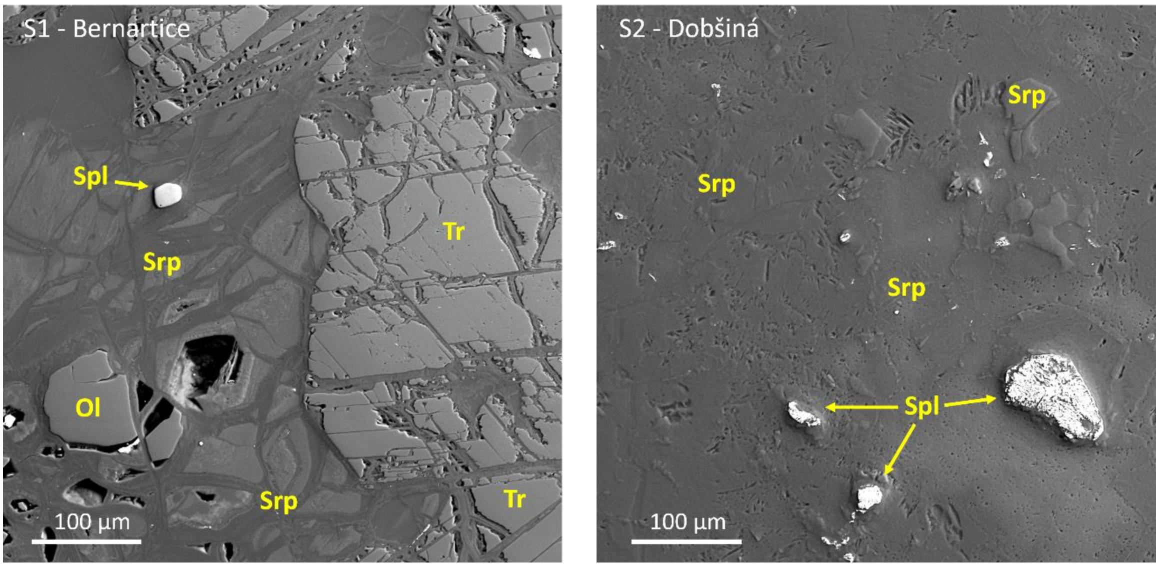

Fig. 7 BSE image of typical microstructure of studied serpentinites. In S1, numerous relicts of primary mineral association and their advanced alteration by secondary serpentine is visible. In S2, serpentine is the dominant mineral phase with only Cr-spinel-magnetite relicts present.

alteration of the original peridotites by newly formed minerals of the serpentinite group can be observed, nevertheless, with relics of the former minerals (such as olivine Fo90 and tremolite) still present. In sample S2, almost no relics were preserved. The replacement of Cr-spinelides by magnetite can be observed in a similar way (Fig. 7). However, it should be noted that the weathering of the serpentinite body affected the overall concentration of trace metals, leading to chemical discrepancies between different profiles.

3.3. RAMAN SPECTROSCOPY ANALYSIS

Micro-Raman spectroscopy is an ideal and reliable technique for determining and differentiating present silicates, oxides or carbonates and distinguishing individual phases within mineral solid solution systems. Most significantly, minor changes between composition and structure can be observed if the solid solutions contain crystal-bound water (e.g., see Novák et al., 2023). Based on this observation, minerals of the serpentine group can be distinguished, where the contained OH can serve as a point of reference in the form of Raman bands in the regions from 3600 to 3800 cm^{-1} (Hajjar et al., 2016, Rizzo et al., 2023).

In the Raman spectra of serpentine minerals (belonging to the phyllosilicate group) in S1 and S2 (Fig. 10), shifts can be observed for Si-O$_b$-Si stretching and SiO_4 bending modes, which occur at 691 and 387 cm^{-1} in chrysotile, 685 and 377 cm^{-1} in antigorite and at 689 and 381 cm^{-1} in serpentine-lizardite, respectively. For antisymmetric Si-O$_b$-Si, a characteristic peak at 1043 cm^{-1} in antigorite could be observed. Other low-frequency modes vary from 100 to 230 cm^{-1} and should be related either to lattice or MO_6 vibration modes. Because the structure reflects the compositional changes, some OH bands detected vary, where chrysotile is characterised by one strong peak at 3694 cm^{-1}, antigorite by peaks ranging between 3660-3698 cm^{-1} and serpentine-lizardite ranging from 3680 to 3701 cm^{-1}. (Groppo et al., 2006, Wang et al., 2015, Lahondère et al., 2019, Aspiotis et

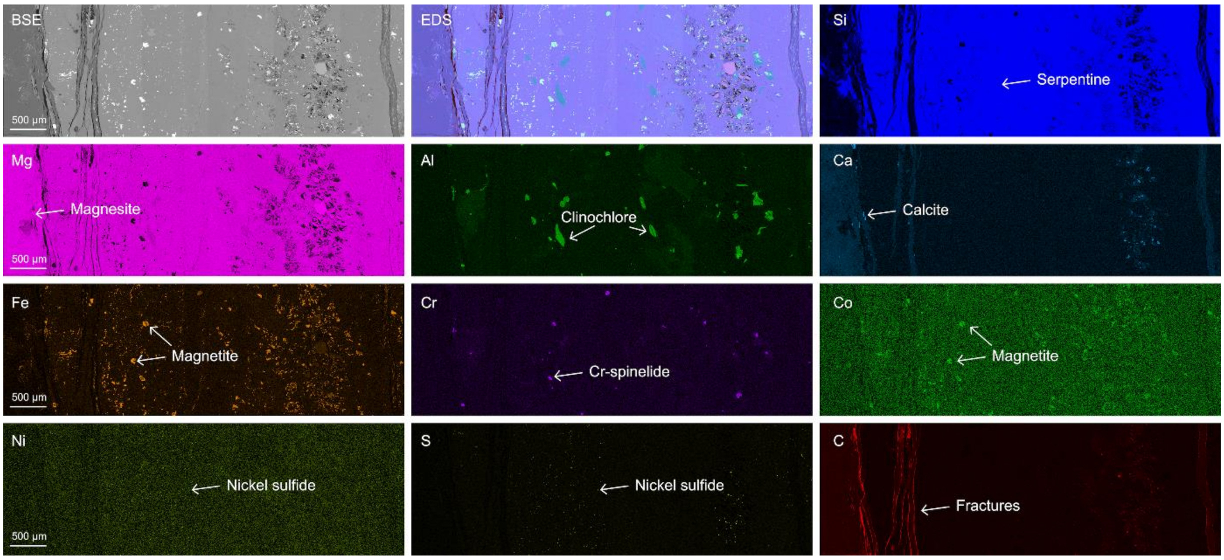

Fig. 8 Compilation of BSE and EDS images with separately listed detected elements bound to specific minerals related to aggregate from Czech serpentinite (S1).

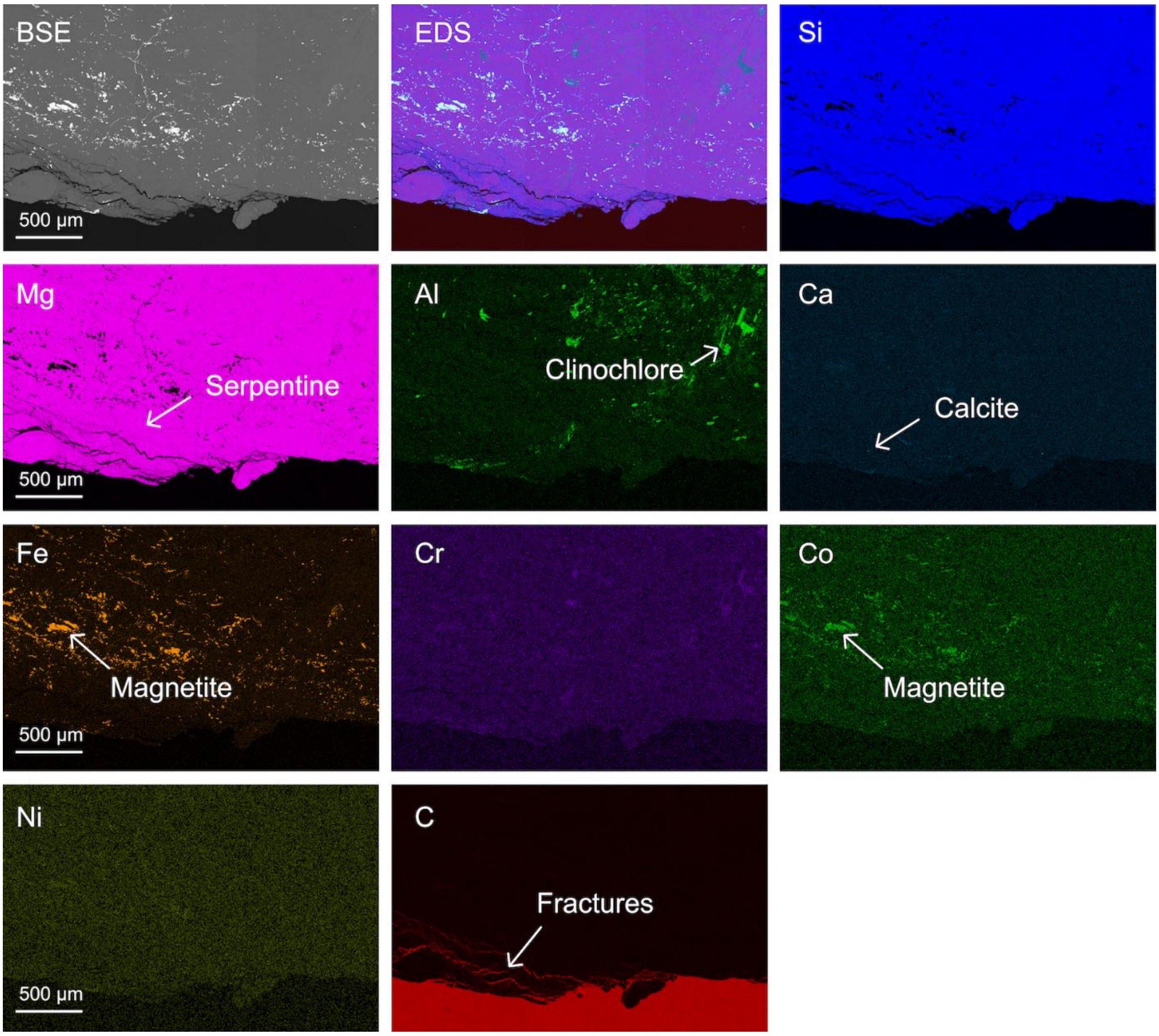

Fig. 9 Compilation of BSE and EDS images with separately listed detected elements bound to specific minerals related to aggregate from Slovak serpentinite (S2).

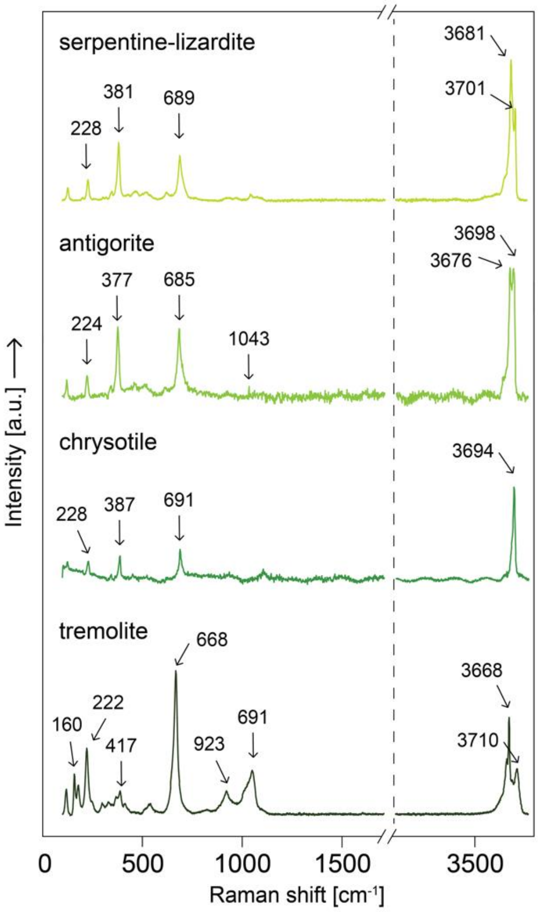

Fig. 10 Comparison of Raman spectra and OH regions of serpentine group minerals (lizardite, antigorite, chrysotile) and tremolite measured in samples S1 and S2, respectively.

al., 2023). For comparison, tremolite is also included here, which has a different spectrum as it structurally belongs to the amphibolite group (Rösche et al., 2022). Antigorite was detected only in S2; altogether, with SEM-EDS analyses, we may establish in Dobšiná a different degree of serpentinization most likely related to mantle wedge (Soda and Wenk, 2014).

In both samples, we were able to identify calcite based on the translational and rotational lattice modes 155 cm^{-1} and 281 cm^{-1} and two internal modes, such as in-plane bending mode v_4 712 cm^{-1} and typical symmetric stretch v_1 around 1086 cm^{-1}. The magnesite spectrum was different (Fig. 11a) with translational and rotational lattice modes at 211 cm^{-1} and 328 cm^{-1}, and two internal modes, such as in-plane bending mode v_4 738 cm^{-1} and dominant symmetric stretch band v_1 around 1094 cm^{-1} (Frezzoti et al., 2012).

Small changes in the spectra of magnetite and the detection of magnesiochromite with characteristic bands in the region 100-800 cm^{-1} are also visible in samples S1 and S2, indicating substitutional changes within the magnetite-chromite spinelide group (See Fig. 11b). These changes belong to the most prevalent band between 650-710 cm^{-1} and are most likely attributed to the $^{M}BO_6$ group (B=Cr, Al, Fe^{3+}) as symmetric stretching vibration v_1. Other bands below 600 cm^{-1} should belong to the v_4 or E_g symmetric ^{M}B–O stretching vibrations (Kharbish, 2018; Krolop et al., 2019).

Another mineral detected using Raman spectroscopy was olivine, which, based on the band positions, will have a chemical composition between the forsterite and fayalite solid solution system with a tendency towards the forsterite component (Kuebler et al., 2006). According to SEM-EDS data, the mineral containing the most aluminium was identified as clinochlore, with three well-defined peaks related to OH vibrations (Fig. 11c), even though the exact peak positions are widely variable. In previous studies, establishing exact vibrations in the chlorite group minerals is quite challenging, as different proportions of Mg^{2+} and Fe^{2+} in the structure may result in complex peak shifts in most Raman bands (Arbiol and Layne, 2021).

4. CONCLUSIONS

In conclusion, the degree of serpentinization and place of a given serpentinite deposit affects the quality of aggregate based on mineral and chemical composition. Based on these differences between samples from the Czech Republic and Slovakia, we addressed changes in composition for elements such as Co, Cr, or Ni. The presence of Co is undesirable, but it is present in only trace amounts in the aggregates, and its proposed quantitative limits can be calculated by numerical modelling, considering the tendency of activation susceptibility and the time required to reach the clearance level. To ensure a longer life of concrete used in NPPs, we recommend using serpentinite with as little cobalt as possible, which may also affect radioactive waste management after the decommissioning of NPPs.

Based on our observation and taking these reasons into account, Slovak serpentinite appears to be less suitable, especially because of the presence of undesirable elements and asbestos. The Czech serpentinite aggregates containing a large proportion of relict minerals such as olivine, pyroxene, and amphibole might also be considered less suitable, as these minerals can significantly contribute to the formation of RIVE during long-term radiation exposure. Nevertheless, when comparing the advantages and disadvantages, Czech serpentinite is a more suitable material for radiation-shielding concrete in general, provided that aggregate quality control is carried out during the selection process and areas with a high degree of serpentinization are prioritised.

Another recommendation is using serpentinite, which is not contaminated with carbonates, as this attribute can also significantly impact the quality and durability of radiation-shielding concrete. Serpentinite should be processed so the calcite or magnesite presence is reduced to a minimum as far as is technologically possible to achieve a high consistency within the aggregate quality. However, for a deeper understanding of other processes within the minerals

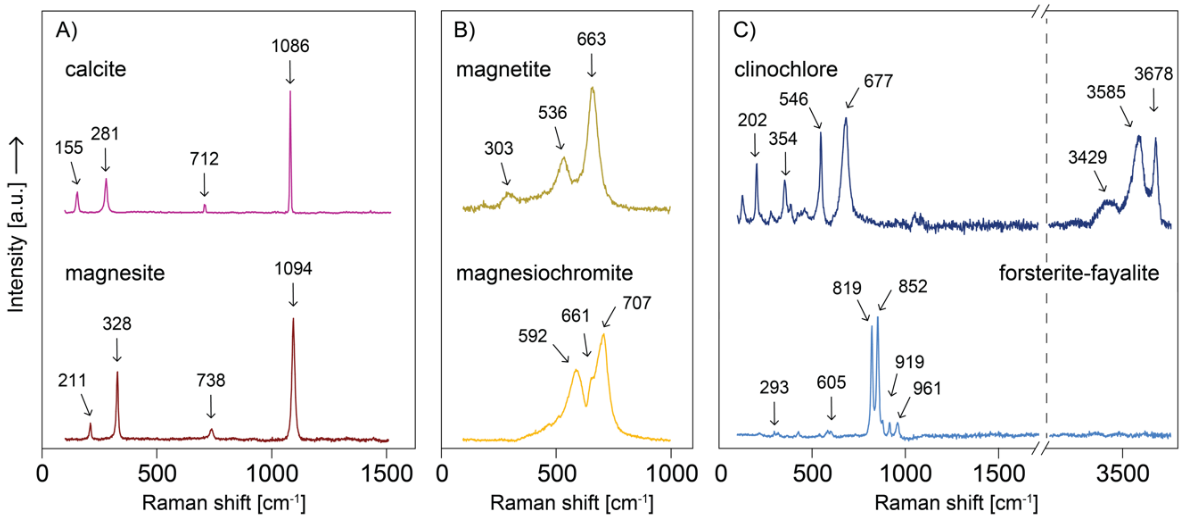

Fig. 11 A collection of spectra of other detected minerals with a) calcite in comparison to magnesite, b) magnetite in comparison to magnesiochromite, and c) clinochlore with distinct OH region in comparison to olivine without the presence of OH vibration.

of the serpentinite group and their exact response to irradiation, it is necessary to carry out further research that includes irradiation in the reactor in the future.

ACKNOWLEDGEMENTS

We are very grateful to Vítězslav Jánský for precision sample preparation. The authors would like to thank anonymous reviewers for improving the quality of this paper. The presented work has been realized within Institutional Support by Ministry of Industry and Trade of the Czech Republic (23D0044) as well as the presented results were obtained using the CICRR infrastructure, which is financially supported by the Ministry of Education, Youth and Sports - project LM2023041 (23D0001).

DECLARATIONS

Competing Interests

The authors have no conflicts of interest to declare that they are relevant to the content of this article.

Author Contributions

All authors contributed to the study's conception and design. Kamil Sobek, Jitka Klaisnerová, Claudia Aparicio and Patricie Halodová performed data collection and analysis. Kamil Sobek wrote the first draft of the manuscript, and all authors commented on previous versions. All authors read and approved the final manuscript.

SUPPLEMENTARY INFORMATION

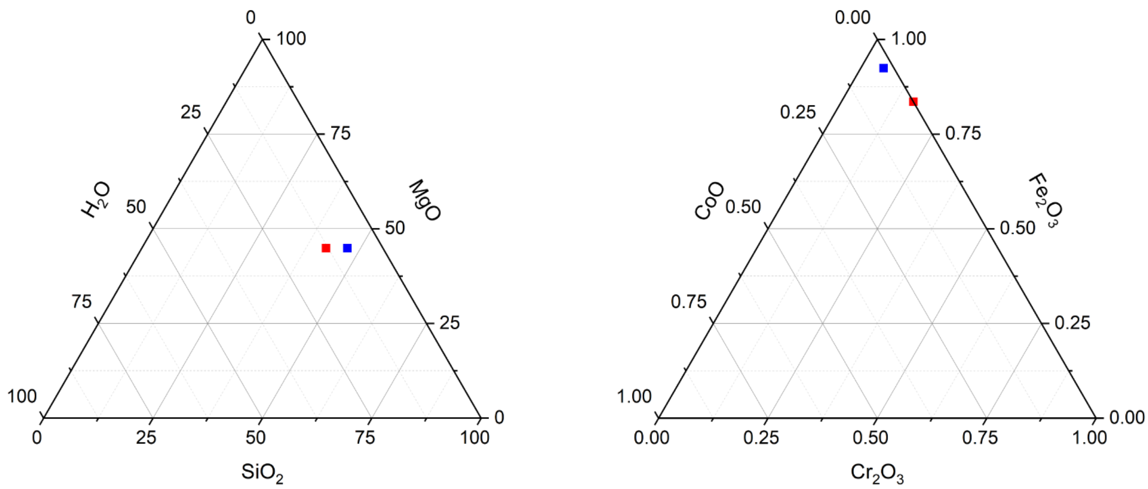

Fig. S1 Ternary diagrams showing the composition of the selected serpentinites, where the red square belongs to S1, and the blue square belongs to S2.

REFERENCES

Abdullah, M.A.H., Rashid, R.S.M., Amran, M., Hejazii, F., Azreen, N.M., Fediuk, R., Voo, Y.L., Vatin, N.I. and Idris, M.I.: 2022, Recent trends in advanced radiation shielding concrete for construction of facilities: Materials and Properties. Polymers, 14, 14, 2830. DOI: 10.3390/polym14142830

Aparicio, C., Rosnecký, V. and Halodová, P.: 2024, Simple preparation of specimens for X-ray powder diffraction analysis of radioactive materials: an illustrative example on irradiated granite. Powder Diffr., 39, 2, 1-6. DOI: 10.1017/S088571562400006X

Arbiol, C. and Layne, G.D.: 2021, Raman spectroscopy coupled with reflectance spectroscopy as a tool for the characterization of key hydrothermal alteration minerals in epithermal Au–Ag systems: Utility and implications for mineral exploration. Appl. Spectrosc., 75, 12, 1475–1496. DOI: 10.1177/00037028211047869

Aspiotis, S., Schlüter, J., Hildebrandt, F. and Mihailova, B.: 2023, Raman spectroscopy for crystallochemical analysis of Mg-rich layered silicates: Serpentine and talc. J. Raman Spectrosc., 54, 12, 1502–1516. DOI: 10.1002/jrs.6601

Beneš, K.: 1963, Explanatory notes to the comprehensive geological map of the Czechoslovak Socialist Republic 1: 200,000: M-33-XXII. Geofond of the Czechoslovak Academy of Sciences Publishing House, Jihlava, 200 pp., (in Czech).

Bruck, P.M., Esselman, T.C., Elaidi, B.M., Wall, J.J. and Wong, E.L.: 2019, Structural assessment of radiation damage in light water power reactor concrete biological shield walls. Nucl. Eng. Des., 350, 9–20. DOI: 10.1016/j.nucengdes.2019.04.027

Caillaud, J., Proust, D., Philippe, S., Fontaine, C. and Fialin, M.: 2009, Trace metals distribution from a serpentinite weathering at the scales of the weathering profile and its related weathering microsystems and clay minerals. Geoderma, 149, 3-4, 199–208. DOI: 10.1016/j.geoderma.2008.11.031

Calzada, E., Grünauer, F., Schillinger, B. and Türck, H.: 2011, Reusable shielding material for neutron-and gamma-radiation. Nucl. Instrum. Methods Phys. Res. A, 651, 1, 77–80. DOI: 10.1016/j.nima.2010.12.239

Coleman, R.G.: 1971, Petrologic and geophysical nature of serpentinites. Geol. Soc. Am. Bull., 82, 4, 897–918. DOI: 10.1130/0016-7606(1971)82

Copinger, D.A., Oland, C.B. and Naus, D.: 2012, A summary of aging effects and their management in reactor spent fuel pools, refueling cavities, tori, and safety-related concrete structures. US Nuclear Regulatory Commission, Office of Nuclear Reactor Regulation.

Dąbrowski, M., Jóźwiak-Niedźwiedzka, D., Bogusz, K. and Glinicki, M.A.: 2022, Influence of serpentinite aggregate on the microstructure and durability of radiation shielding concrete. Constr. Build. Mater., 337, 127536. DOI: 10.1016/j.conbuildmat.2022.127536

Deer, W.A., Howie, R.A. and Zussman, J.: 2009, Rock Forming Minerals: Layered Silicates Excluding Micas and Clay Minerals. Geological Society of London.

Denisov, A., Dubrovskii, V. and Solovyov, V.: 2012, Radiation resistance of mineral and polymer construction materials. ZAO MEI Publ. House.

Denisov, A.: 2018, Radiation changes in serpentinite concretes of "dry" radiation shield in nuclear power plants. IOP Conf. Ser.: Mater. Sci. Eng. 365 032028. DOI: 10.1088/1757-899X/365/3/032028

Frezzotti, M.L., Tecce, F. and Casagli, A.: 2012, Raman spectroscopy for fluid inclusion analysis. J. Geochem. Explor., 112, 1–20. DOI: 10.1016/j.gexplo.2011.09.009

Groppo, C., Rinaudo, C., Cairo, S., Gastaldi, D. and Compagnoni, R.: 2006, Micro-Raman spectroscopy for a quick and reliable identification of serpentine minerals from ultramafics. Eur. J. Mineral., 18, 3, 319-329. DOI: 10.1127/0935-1221/2006/0018-0319

Hajjar, Z., Wafik, A., Constantin, M. and Bhilisse, M.: 2016, Process of serpentinization in the ultramafic massif of Beni Bousera (internal Rif, Morocco). Arab. J. Geosci., 9, 1–9. DOI: 10.1007/s12517-016-2507-6

Hodel, F., Macouin, M., Triantafyllou, A., Carlut, J., Berger, J., Rousse, S., Ennih, N. and Trindade, R.I.F.D.: 2017, Unusual massive magnetite veins and highly altered Cr-spinels as relics of a Cl-rich acidic hydrothermal event in Neoproterozoic serpentinites (Bou Azzer ophiolite, Anti-Atlas, Morocco). Precambrian Res., 300, 151–167. DOI: 10.1016/j.precamres.2017.08.005

Hovorka, D., Jaroš, J., Kratochvíl, M. and Mock, R.: 1984, The Mesozoic ophiolites of the Western Carpathians. Krystalinikum, 17, 143–157.

Hovorka, D., Ivan, P., Jaroš, J., Kratochvíl, M., Reichwalder, P., Rojkovič, I., Spišiak, J. and Turanová, L.: 1985, Ultramafic rocks of the Western Carpathians, Czechoslovakia. Geological Institute of Dionýz Štúr Publishers, Bratislava, Czechoslovakia, 258 pp.

Kharbish, S.: 2018, Raman spectroscopic features of Al-Fe^{3+}- poor magnesiochromite and Fe^{2+}-Fe^{3+}-rich ferrian chromite solid solutions. Mineral. Petrol., 112, 245–256. DOI: 10.1007/s00710-017-0531-1

Khmurovska, Y. and Štemberk, P.: 2021, Catalogue of radiation-induced damage of rock aggregates identified by RBSM analysis. J. Adv. Concr. Technol., 19, 6, 668–686. DOI: 10.3151/jact.19.668

Krolop, P., Jantschke, A., Gilbricht, S., Niiranen, K. and Seifert, T.: 2019, Mineralogical imaging for characterization of the per geijer apatite iron ores in the Kiruna District, Northern Sweden: a comparative study of mineral liberation analysis and raman imaging. Minerals, 9, 9, 544. DOI: 10.3390/min9090544

Kuebler, K.E., Jolliff, B.L., Wang, A. and Haskin, L.A.: 2006, Extracting olivine (Fo–Fa) compositions from Raman spectral peak positions. Geochim. Cosmochim. Acta, 70, 24, 6201–6222. DOI: 10.1016/j.gca.2006.07.035

Lahondère, D., Cagnard, F., Wille, G. and Duron, J.: 2019, Naturally occurring asbestos in an alpine ophiolitic complex (northern Corsica, France). Environ. Earth Sci., 78, 1–23. DOI: 10.1007/s12665-019-8548-x

Lavdanskij, P.A., Nazarov, V.M., Stefanov, N.I. and Frontasyeva, M.V.: 1989, Neutron activation analysis for determination of induced radioactivity in concrete of nuclear reactor shielding. J. Radioanal. Nucl. Chem., 131, 261–270. DOI: 10.1007/BF02060591

Maruyama, I., Kontani, O., Takizawa, M., Sawada, S., Ishikawao, S., Yasukouchi, J., Osamu, S., Etoh, J. and Igari, T.: 2017, Development of soundness assessment procedure for concrete members affected by neutron and gamma-ray irradiation. J. Adv. Concr. Technol., 15, 9, 440–523. DOI: 10.3151/jact.15.440

Masoud, M.A., Kansouh, W.A., Shahien, M.G., Sakr, K., Rashad, A.M. and Zayed, A.M.: 2020, An experimental investigation on the effects of barite/hematite on the radiation shielding properties of serpentine concretes. Prog. Nucl. Energy, 120, 103220. DOI: 10.1016/j.pnucene.2019.103220

Meer, F.V.D.: 1994, Mapping the degree of serpentinization within ultramafic rock bodies using imaging spectrometer data. Int. J. Remote Sens., 15, 18, 3851–3857. DOI: 10.1080/01431169408954364

Moody, J.B.: 1976, Serpentinization: a review. Lithos, 9, 2, 125–138. DOI: 10.1016/0024-4937(76)90030-X

Novák, M., Dolníček, Z., Zachař, A., Gadas, P., Nepejchal, M., Sobek, K., Škoda, R. and Vrtiška, L.: 2023, Mineral assemblages and compositional variations in bavenite–bohseite from granitic pegmatites of the Bohemian Massif, Czech Republic. Mineral. Mag., 87, 3, 415–432. DOI: 10.1180/mgm.2023.17

Olsen, A.A., Bodkin, M.A. and Hausrath, E.M.: 2023, Quantifying early mineral weathering reactions in serpentinite bedrock. Appl. Geochem., 148, 105543. DOI: 10.1016/j.apgeochem.2022.105543

Pauliš, P. and Ďuďa, R.: 2002, The most interesting mineralogical localities of Slovakia. Kutná Hora. Kuttna, 136 pp. (in Czech).

Pauliš, P., Veselovský, F., Kadlec, T. and Franc, J.: 2010, Huntite from the quarry at Bernartice near Dolní Kralovice (Czech Republic). Bull. Mineral.-petrolog. Odd. Nár. Muz. (Praha), 18, 1, 85–88, (in Czech).

Piotrowski, T.: 2021, Neutron shielding evaluation of concretes and mortars: A review. Constr. Build. Mater., 277, 122238. DOI: 10.1016/j.conbuildmat.2020.122238

Remec, I., Field, K.G., Naus, D.J., Rosseel, T.M. and Busby, J.T.: 2013, Concrete aging and degradation in NPPs: LWRS program RandD progress report. In: 2013 ANS Winter Meeting and Nuclear Technology Expo, 403–406.

Rizzo, G., Buccione, R., Dichicco, M., Punturo, R. and Mongelli, G.: 2023, Petrography, geochemistry and mineralogy of serpentinite rocks exploited in the ophiolite units at the Calabria-Basilicata Boundary, Southern Apennine (Italy). Fibers, 11, 10, 81. DOI: 10.3390/fib11100081

Rösche, C., Waeselmann, N., Petrova, N., Malcherek, T., Schlüter, J. and Mihailova, B.: 2022, Oxidation processes and thermal stability of actinolite. Phys. Chem. Miner., 49, 12, 47. DOI: 10.1007/s00269-022-01223-4

Rüpke, L.H., Morgan, J.P., Hort, M. and Connolly, J.A.: 2004, Serpentine and the subduction zone water cycle. Earth Planet. Sci. Lett., 223, 1-2, 17–34. DOI: 10.1016/j.epsl.2004.04.018

Sengupta, A., Rajeswari, B., Kadam, R. and Kshirsagar, R.: 2012, Characterization of serpentine: a potential nuclear shielding material. J. Radioanal. Nucl. Chem., 292, 2, 903–908. DOI: 10.1007/s10967-011-1535-7

Sobolev, N.V. and Logvinova, A.M.: 2005, Significance of accessory chrome spinel in identifying serpentinite paragenesis. Int. Geol. Rev., 47, 1, 58-64. DOI: 10.2747/0020-6814.47.1.58

Soda, Y. and Wenk, H.R.: 2014, Antigorite crystallographic preferred orientations in serpentinites from Japan. Tectonophysics, 615, 199–212. DOI: 10.1016/j.tecto.2013.12.016

Toft, P.B., Arkani-Hamed, J. and Haggerty, S.E.: 1990, The effects of serpentinization on density and magnetic susceptibility: a petrophysical model. Phys. Earth Planet. Inter., 65, 1-2, 137–157. DOI: 10.1016/0031-9201(90)90082-9

Torrenti, J.M. and Nahas, G.: 2010, Durability and safety of concrete structures in the nuclear context. In: Proc. 6th International Conference on Concrete under Severe Conditions (CONSEC'10), Merida, Yucatan, Mexico, 3–18. DOI: 10.1201/b10552-3

Wang, A., Freeman, J.J. and Jolliff, B.L.: 2015, Understanding the Raman spectral features of phyllosilicates. J. Raman Spectrosc., 46, 10, 829–845. DOI: 10.1002/jrs.4680